J. Geophys. Res., 1998

Retrieval of stratospheric temperatures from space borne microwave limb sounding measurements

T. Wehr[1], S. Bühler, A. von Engeln, K. Künzi

Institute of Remote Sensing, University of Bremen, Germany

J. Langen

ESA-ESTEC, Noordwijk, The Netherlands

Abstract.
Microwave limb sounding is a well suited technique for the observation of the composition and temperature of the middle atmosphere. The shuttle-borne Millimeter-Wave Atmospheric Sounder (MAS) measures three oxygen lines in the 61-64 GHz region. Since oxygen is uniformly mixed in the lower and middle atmosphere, the amplitude and shape of the emission lines depends only on temperature and pressure. From these oxygen emission lines vertical temperature profiles are retrieved with a vertical resolution of 5 km in the altitude region of 15-45 km (127-1.5 hPa). The estimated total error is 1.5 K at altitudes of 25-35 km (24.5-5.7 hPa) and up to 5 K above and below this region. Simultaneously with the temperature profile certain instrument parameters are retrieved. We present the first MAS temperature retrieval results taken at three different locations from measurements of 31 March 1992 during the ATLAS-1 mission. The temperature retrieval results are basically in good agreement with National Center for Environmental Prediction (NCEP) analysis data, but the MAS retrievals have the tendency to low temperatures in the lower stratosphere.

Introduction

Space borne microwave receivers can be used for global measurements of atmospheric composition and temperature. The MAS is a passive millimeter-wave limb sounding radiometer, which measures atmospheric radiance in order to retrieve profiles of O_3, H_2O, ClO, temperature and pressure simultaneously. It operates on board the space shuttle and has been flown three times as part of the ATLAS (Atmospheric Laboratory for Application and Science) mission from 1992 to 1994. The main objective of the ATLAS mission is to study the photo chemistry and dynamics of the stratosphere and mesosphere. The ATLAS mission has been described by *Kaye et al.,* [1996].

Results of ozone, water vapor and ClO of MAS measurements in the middle atmosphere have been published by *Hartmann et al.* [1996 b]. Additional MAS measurements have been published about ozone retrievals in the high-altitude stratosphere [*Olivero et al.*, 1996], mesospheric and lower thermospheric water vapor and ozone [*Bevilacqua et al.*, 1996], upper stratospheric ClO [*Aellig*, 1996 a] and arctic stratospheric and mesospheric H_2O [*Aellig*, 1996 b]. Some preliminary results of temperature retrievals have been published by *Wehr et al.* [1997].

Other retrievals of temperature profiles from measurements by space borne microwave instruments have been published, for example from the NEMS instrument on NIMBUS 5 Microwave Satellite [*Waters et al.* , 1975] and the UARS Microwave Limb Sounder [*Fishbein et al.* , 1996].

[1]Now at University of Maryland Baltimore County, USA

The focus of this paper is to present stratospheric temperature retrieval results of the ATLAS-1 mission. The retrieved parameters are the temperature (T) and pressure (p) profile, assuming hydrostatic balance. Critical instrument parameters are also simultaneously retrieved, as described below. Finally, the temperature retrieval results were compared to the National Center for Environmental Prediction (NCEP) analysis. Both data sets are found to be in agreement within the MAS retrieval error bars.

The MAS Instrument

The MAS operates on board the space shuttle at an altitude of about 300 km. The orbit inclination is 57°. The field of view is perpendicular to the flight direction. Depending on the yaw orientation of the shuttle, the latitudinal coverage of the measurement is 70° N to 40° S or 40° N to 70° S. The duration of one MAS scan cycle corresponds to a ground distance of about 100 km.

The details of the MAS instrument are described by *Croskey et al.* [1992]. The MAS is a sensor which contains three separate microwave radiometers using heterodyne technique. One radiometer measures the oxygen lines 9+ (61.151 GHz), 15+ (62.998 GHz) and 17+ (63.568 GHz), a second radiometer measures H_2O at 183.310 GHz and O_3 at 184.377 GHz, and a third radiometer measures ClO at 204.352 GHz.

The oxygen lines are observed to derive atmospheric p and T profiles. From the same lines critical instrument parameters are retrieved, since they are not known accurately enough. These parameters are described in the subsection "retrieval of instrument parameters".

The MAS scans the limb of the atmosphere by a continuous movement of the antenna through the tangent point altitude range of about 5 to 130 km. One limb scan consists of a continuous down- and an up-movement of the antenna, plus calibration positions. The total time for one cycle is 12.8 s, immediately followed by the next cycle. 320 single spectra are integrated during one cycle, with a data sample interval (DSI) of 0.04 s. The antenna angle and shuttle position is given for each DSI.

The line spectrum of O_2 around 60 GHz is the result of spin flip transitions at different rotational levels. The spin S results from two unpaired electrons adding up to $S = 1$ for the O_2 molecule. The orbital angular momentum is zero and the spin angular momentum is coupled to the rotational angular momentum through a weak magnetic field arising from the molecular rotation. The Zeeman splitting due to the earth magnetic field affects the center of the oxygen lines [*Hartmann et al.*, 1996 a]. Since the forward model currently ignores Zeeman splitting, we cannot use the line center for the retrievals. Each oxygen line is observed with a bandwidth of 400 MHz, from which we disregard ± 10 MHz from the center frequency, which is a conservative estimate. Consequently, we cannot retrieve mesospheric temperatures. In this analysis we focus on temperature and pressure in the stratosphere.

Retrieval Technique

The forward model F calculates the received spectral power vector $\mathbf{y} = F(\mathbf{x}, \mathbf{b})$, using the radiative transfer equation. It also models the instrument characteristics. $\mathbf{b}$ are the model data, which are assumed to be sufficiently known and $\mathbf{x}$ are the parameters which have to be retrieved. In our analysis, $\mathbf{x}$ consist of the temperature profile and specific instrument parameters, as described below. $\mathbf{b}$ contains all other model parameters, e.g., the spectroscopic data base.

The inverse model I returns the best estimate of $\mathbf{x}$, which is named $\hat{\mathbf{x}}$. I is a function of the measurement $F(\mathbf{x}, \mathbf{b}) + \epsilon_y$ (where ϵ_y is the measurement noise), the constant model parameter $\mathbf{b}$ and a priori data $\mathbf{c}$:

$$\hat{\mathbf{x}} = I(F(\mathbf{x}, \mathbf{b}) + \epsilon_y, \hat{\mathbf{b}}, \mathbf{c}) \tag{1}$$

where $\hat{\mathbf{b}}$ is the best estimate of the true model parameter $\mathbf{b}$. In this analysis we assume $\hat{\mathbf{b}} = \mathbf{b}$, since the errors in $\hat{\mathbf{b}}$ are small. The most critical elements of $\mathbf{b}$ are the spectroscopic data. We use the oxygen line parameters published by *Liebe et al.* [1992], given with an error estimate for the absorption coefficient of 2%.

We can approximate the forward model $F(\mathbf{x})$ by a Taylor series

$$\mathbf{y} = F(\mathbf{x}_0) + \frac{\partial F}{\partial \mathbf{x}}(\mathbf{x} - \mathbf{x}_0) = \mathbf{y}_0 + \mathbf{K}_0(\mathbf{x} - \mathbf{x}_0) \tag{2}$$

where $\partial F / \partial \mathbf{x} = \mathbf{K}$ is the Jacobian matrix of F and $\mathbf{x}_0$ is the linearization point, for which we use the a priori. The optimal estimation method with Newtonian iteration [*Rodgers*, 1976] has been selected for our retrievals. We obtain the iterative retrieval formula for the $(n+1)$-th iteration:

$$\begin{aligned} \mathbf{x}_{n+1} &= \mathbf{x}_0 + (\mathbf{S}_0^{-1} + \mathbf{K}_n^T \mathbf{S}_y^{-1} \mathbf{K}_n)^{-1} \mathbf{K}_n^T \mathbf{S}_y^{-1} \\ &\quad \cdot [(\mathbf{y} - \mathbf{y}_n) - \mathbf{K}_n(\mathbf{x}_0 - \mathbf{x}_n)] \end{aligned}$$

where T denotes the matrix transpose, $\mathbf{y}_n$ is a synthetic spectrum, calculated from the n-th iteration result $\mathbf{x}_n$. $\mathbf{x}_0$ is the a priori, $\mathbf{S}_y$ is the noise covariance matrix

of the measured spectrum, given by the instrument's noise, $\mathbf{S}_0$ is the a priori error covariance matrix, which represents the uncertainty of the a priori assumptions. As the convergence criterion we use the residual of $\mathbf{x}_{n+1}$ and $\mathbf{x}_n$.

The statistical error covariance matrix of the last iteration is called $\hat{\mathbf{S}}$. It can be calculated as

$$\hat{\mathbf{S}} = (\mathbf{S}_0^{-1} + \hat{\mathbf{K}}^T \mathbf{S}_y^{-1} \hat{\mathbf{K}})^{-1} \tag{3}$$

by using the Jacobian matrix $\hat{\mathbf{K}}$, which has been calculated with the result of the last iteration. $\hat{\mathbf{S}}$ is the sum of the smoothing error covariance matrix and the measurement error covariance matrix, which both can be calculated separately. The smoothing error covariance matrix represents the retrieval parameter errors due to smoothing between the retrieval parameters, e.g., vertical smoothing of the temperature profile. The measurement error covariance matrix represents the error in the retrieved parameters due to statistical errors (noise) in the measured spectrum.

The a priori data are the first guess of the retrieval parameters and the start point of the iterative retrieval procedure. The a priori temperature profile and surface pressure are taken from an atmosphere model. The a priori data of the instrument's parameters, which shall be retrieved, are taken from the instrument's specifications or a previous analysis by *Berg* [1996].

The statistical errors are calculated for each retrieval. A very useful tool to assess the quality of a retrieval is the averaging kernel matrix

$$\mathbf{A} = (\partial I/\partial \mathbf{y}) \cdot (\partial F/\partial \mathbf{x}) \tag{4}$$

which represents the sensitivity of the retrieval to the retrieval parameters. If the corresponding averaging kernel matrix element of a retrieval parameter is large (≈ 1), the retrieval is sensitive to this parameter. If it is close to zero the retrieved value is dominated by the a priori assumption. The widths of the rows of the averaging kernel matrix represent the smoothing of the retrieved parameters. An example of the averaging kernel matrix will be given later.

With the definition of the averaging kernel matrix we can write the mathematical definition of the smoothing error covariance matrix as

$$\mathbf{S}_N = (\mathbf{A} - \mathbf{I})\mathbf{S}_0(\mathbf{A} - \mathbf{I})^T \tag{5}$$

where $\mathbf{I}$ is the unit matrix. The measurement error covariance matrix is defined by

$$\mathbf{S}_M = \mathbf{D}_y \mathbf{S}_y \mathbf{D}_y^T \tag{6}$$

with

$$\mathbf{D}_y = \frac{\partial I}{\partial \mathbf{y}} \tag{7}$$

$\mathbf{D}_y$ is the Jacobian matrix of the retrieval I with respect to the measurement vector $\mathbf{y}$. The total statistical error covariance matrix of the retrieved parameters is the sum of $\mathbf{S}_N$ and $\mathbf{S}_M$ which is identical to $\hat{\mathbf{S}}$ in equation (3).

A detailed description of retrieval techniques, retrieval software and analysis of synthetic measurements is given by *Wehr* [1996].

Retrieval of Atmospheric Parameters

The independent coordinate in our retrievals is the geometrical altitude. The reason for choosing the geometrical altitude is more of historical nature, because the tangent point of the antenna beam is geometrically calculated by the antenna angle and the position coordinates of the shuttle navigation system. Therefore, the calibrated spectra of each scan angle are provided for the retrieval system together with the antenna scan angle and the tangent point altitude.

Whether the independent coordinate of the retrieval is altitude or pressure does not matter at all, because we assume a hydrostatic atmosphere and assume to know the surface pressure. For the radiative transfer calculations we need both the pressure and the altitude, the latter for optical path length calculation. For the a priori temperature profile we use atmosphere model data after *Fleming et al.* [1988]. This data set contains temperatures and pressures as a function of the geometrical altitude. In this data set pressure values are not given for altitudes below 20 km. Also, these atmosphere data are not hydrostatic. Therefore we take the pressure value at 20 km and calculate the hydrostatic pressure profile upwards and downwards by using the hydrostatic equation

$$p(z) = p(z_0) \exp\left(-\int_{z_0}^{z} \frac{g(z')M}{RT(z')} dz' \right) \tag{8}$$

where $p(z)$ is the pressure at the altitude z, $p(z_0)$ is the pressure at an altitude $z_0 < z$, $g(z')$ is the earth's gravitation at altitude z', $T(z')$ is the temperature at z', M is the air molecular mass, R is the universal gas constant. This gives us the a priori atmosphere with pressures and temperatures on a geometrical altitude grid.

The first retrieval iteration calculates new temperatures on the given altitudes with the optimal estimation method described above. Afterwards, the hydrostatic

equation (8) is used to recalculate the pressure profile for the new temperatures at the given altitudes. For this, we use the surface pressure of the a priori profile. The new atmosphere profile therefore consists of the altitudes (which never changes), the retrieved temperatures (using the optimal estimation method) and the recalculated pressures (using equation 8). All following retrieval iterations do the same procedure of retrieving the temperatures and recalculating the pressures afterwards. The surface pressure derived from the a priori profile does not change. Note, that the a priori vector $\mathbf{x}_0$ in the optimal estimation equations contains the temperatures of the a priori, but not the pressures.

Theoretically, it is possible, to treat the surface pressure as an additional retrieval parameter. Test calculations have shown that the MAS data do not contain enough information to provide this information and would calculate very unreasonable surface pressure values. Therefore, the surface pressure must be kept constant. The assumption of a certain surface pressure means the assumption of a respective air mass above the surface, because in a hydrostatic atmosphere the surface pressure is caused by the mass of the air above the surface. To treat the surface pressure as a free parameter in the retrieval, means to retrieve the mass of the air above the surface.

The forward calculations are performed on a 1 km altitude grid. The temperatures are retrieved on a vertical grid with 5 km spaced point profile with linear temperature interpolation between the grid points. The 5 km resolution represents approximately the instruments resolution in the stratosphere. The vertical resolution of a limb sounding instrument is determined by the antenna beam width, the pressure broadening of the observed emission lines, the frequency resolution and the signal-to-noise ratio of the receiver. For the MAS the antenna beam width is the dominant parameter.

The data input for a single profile retrieval is one limb-scan (down-scan plus up-scan). Every limb-scan is retrieved separately. No smoothing or averaging between different scans has been applied. All filter bank channels of the three oxygen lines are evaluated simultaneously, weighted by the noise error covariance matrix.

The temperature profile a priori covariance matrix is diagonal, i.e., we do not introduce correlations. All diagonal elements of the temperature a priori covariance matrix are $(5\mathrm{K})^2$, corresponding to $\sigma_T = 5\,\mathrm{K}$, which is a very conservative assumption considering that the vertical spacing is 5 km.

Continuum Emission Continuum emission provides an approximately constant offset over the measured band width for each O_2 line. Since the continuum contamination of the measurement is not known accurately, it has to be processed in the retrieval. A simple way is to subtract a linear base line from each oxygen line for every tangent altitude, from both the measurement and the synthetic spectra. Each base line is defined by the mean value of the brightness temperatures for the observed O_2 line at the wings. This is of course not a continuum retrieval, but a way around continuum emission uncertainties.

This means that we implicitly do not use the absolute values of the measured radiance, which causes information loss, especially around 15 km (127 hPa) and below. We cannot retrieve tropospheric temperatures without an accurate continuum emission model.

Retrieval of Critical Instrument Parameters

Simultaneously with the temperature profiles, critical instrument parameters are retrieved. These parameters are retrieved for every temperature profile in order to monitor changes in their retrieved values by scan cycles and time, even if some of these parameters are not expected to change. All the described critical instrument parameters and the temperature profile are retrieved simultaneously for each scan cycle.

Tangent Point Altitude Because of uncertainties in the shuttle navigation system, the tangent point altitudes, calculated from the scan angle and shuttle navigation system informations, are not accurate.

The altitudes of the antenna beam tangent points have been more accurately retrieved by *Berg* [1996] and *Langen et al.* [1994]. These calculations have been made by fitting the measured MAS spectra to model spectra, calculated with the respective model atmospheres after *Fleming et al.* [1988] for the corresponding latitude and month.

During one limb scan cycle the shuttle performs a slowly constant roll movement, because of the conservation of angular momentum of the shuttle, unless the positioning control system changes the shuttle's angular momentum. This happens about every 12 hours for position stabilization.

We can calculate the correct relative tangent altitudes using the shuttle roll angle and the antenna angle which are given for each data sample interval (DSI, see section "The MAS Instrument"). The absolute tangent altitude is retrieved simultaneously with the temperature profile and the other critical instrument parame-

ters. As an a priori value for the absolute tangent altitude we use the results of *Berg* [1996]. Berg retrieves the tangent altitude separately for each DSI. From his retrieval results we use only the tangent altitude of one DSI per scan cycle, which has a tangent altitude close to 35 km, which is Berg's tangent altitude with the smallest fit error. The tangent altitude value of every other individual DSI of the same scan cycle is calculated from the roll angle and antenna angle information of each individual DSI plus the 35-km-DSI value from Berg. Hence, only one tangent altitude offset number per scan cycle is a retrieval parameter and one of the elements of $\mathbf{x}$ in equation (1).

The differences of our a priori tangent altitudes and the tangent altitudes retrieved with our algorithm are referred to as the tangent altitude offset Δh_{alt}. The retrieval results of Δh_{alt} are a function of both the uncertainties in the shuttle navigation system and the fixed surface pressure, which is taken from the a priori atmosphere profile. A wrong surface pressure causes an altitude shift in the altitude-pressure relation and in Δh_{alt}. Therefore, the absolute value of the retrieved Δh_{alt} is only true if the surface pressure is correct. But even if the surface pressure is wrong, Δh_{alt} is consistent with the calculated altitude-pressure function, which is the important aspect. Because the absolute value of Δh_{alt} depends on the accuracy of the surface pressure, it is only presented for one example retrieval.

Brightness Scaling A careful analysis shows that the received spectral power is smaller than expected, probably due to errors in the antenna characteristics. To compensate for this, a brightness temperature scaling factor of the synthetic spectra, calculated with the forward model, has to be retrieved as an additional parameter. The a priori assumption is a scaling factor of 0.92 after the previous analysis of *Berg* [1996]. It has been tested in a large number of evaluations, that an a priori value of 1.0, which is the expected scaling factor according to the instrument specifications, would result in the same retrieval results.

Sideband Efficiency The MAS is a microwave heterodyne receiver. The measured brightness temperature at the frequency ν, $T_{B,\nu}$, is the sum of the brightness temperatures in the signal band T_ν^S and the image band T_ν^I, weighted with the sideband efficiency s_ν

$$T_{B,\nu} = s_\nu T_\nu^S + (1 - s_\nu) T_\nu^I \qquad (9)$$

This signal composition takes place in the first intermediate frequency range, which is the difference of the frequency of the atmospheric signal and the frequency of the first local oscillator of the MAS. Hence, the sideband efficiency retrieval results will be shown as a function of the intermediate frequency. The sideband efficiencies of the three oxygen lines are assumed to be independent from each other. Within each frequency range of the three oxygen lines, the sideband efficiency is assumed to be a linear function of frequency.

The instrument operates as a double sideband receiver. Because of insufficient ground characterization of the sideband efficiency s_ν, it is retrieved as a linear function of frequency, independently for each of the three O_2 lines. As the first guess (a priori), a double sideband efficiency of $s_\nu = 0.5$ is assumed for all frequencies, corresponding to a perfect double sideband receiver.

Results

The MAS temperatures are presented on a pressure grid, rather than on an altitude grid, even though the altitudes are the independent variables. Since we compare to NCEP data which are available on pressure levels, and not on geometric altitudes. The MAS retrieval results are plotted on the retrieved pressure levels.

Retrieval Result of a Single Measurement

As an example for a retrieval of a single scan cycle we discuss the results of 31 March 1992, measured over the tropical Atlantic Ocean at a mean tangent point position of -20.4° longitude and -7.81° latitude.

Figure 1 shows the retrieved atmospheric temperature profile (above) and the simultaneously retrieved instrument parameters (below). The upper plot shows three different profiles; the MAS retrieval (solid line), the a priori temperature profile after *Fleming et al.* [1988] (dashed) and the NCEP profile (dotted) for comparison.

The a priori and NCEP profiles are in good agreement below 15 km (127 hPa) and between 20-35 km (54-5.7 hPa). In the tropopause and stratopause the NCEP temperatures are below the a priori temperatures. NCEP data were not available above 1 hPa. The reliable altitude range of the MAS retrieval in this example is 15-50 km (127-0.8 hPa).

The MAS temperatures are in very good agreement with the NCEP data. Compared to the NCEP data the MAS results show the lowest tropopause temperature to occur at 15 km (127 hPa). Considering the low vertical resolution of the MAS profile (5 km), this result is still consistent with the NCEP data, which show the lowest temperature around 18 km (75.9 hPa). At the stratopause the MAS retrieval is also in very good agree-

ment with the NCEP data. The influence of the a priori information becomes significant above 50 km (1.5 hPa), and the retrieval becomes similar to the a priori. The surface pressure has been extrapolated from the 20 km (54 hPa) pressure value of the data after *Fleming et al.* [1988]. The retrieval of the temperature profile converges after the second iteration.

The three lower plots in Figure 1 show the results of the instrument parameter retrieval. The leftmost plot shows the sideband efficiency at the first and last frequency of each frequency range, which are given in intermediate frequencies. The sideband efficiency has been retrieved independently for each of the three oxygen lines as a linear function in frequency. The retrieval of these parameters converges after the first iteration and shows that the oxygen radiometer channels are close to a double sideband response. This is consistent with the results from *Berg* [1996].

The lower-middle plot shows the value of the retrieved altitude correction, which is an offset to the a priori data. The retrieved altitude offset is typically in the order of some hundreds of meters and converges rapidly. The brightness temperature scaling factor converges to a value of 0.95. Since this value is also found in the retrievals of the other profiles discussed here, this can be interpreted as a systematic instrumental effect. The instrument hardware has not been checked for this effect, because the required measurements cannot be performed with the instrument in its present configuration. However, the results can be considered reliable, since the same value is consistently evaluated in a large number of retrievals.

The retrieved temperatures are independent from each other in the middle and upper stratosphere and slightly smoothed in the lower stratosphere. The averaging kernels (defined here as the rows of the averaging kernel matrix) of the retrieved temperature profile are given in Figure 2 (right). In the range of 25-45 km (24.5-1.5 hPa) the values are approximately equal to one. Therefore, the temperatures are not influenced by the a priori data. The smoothing effect is small in the range of 25-40 km (24.5-2.9 hPa). Below and above this altitude range the profile is smoothed and slightly influenced by the a priori data. Below 15 km (126.6 hPa) and above 55 km (0.4 hPa) the temperatures are dominated by the a priori data. The error correlation for the temperatures at each grid point (altitude level) is approximately -0.3 to the temperatures at the neighboured vertical grid points, which is small considering that the total precision is around 2 K. The error correlations are derived from the error covariance matrices, which are not shown here. The reason for disappearing averaging kernels below 15 km (127 hPa) is the uncertainty of continuum emission, for which we cannot use the absolute values of the measured radiances. The averaging kernels would not disappear, if we knew the continuum emission. The averaging kernels disappear in the mesosphere because we are not using the inner 20 MHz of the oxygen lines which are affected by Zeeman splitting.

The left plot of Figure 2 shows the statistical error profiles. The total statistical error is a composition of the measurement noise error due to the receiver noise (dashed line) and smoothing errors. Even for the 5 km resolution we still observe a slight vertical smoothing, which is very small in the altitudes where the averaging kernels are close to one (right plot). The statistical error of the MAS temperature profiles varies between 1.5 K and 4 K depending on the altitude.

The averaging kernels and the error profiles are representative for all retrieved profiles presented in this paper. Differences of this retrieval to the retrievals presented below are negligible. For all retrievals shown below we retrieved the same sideband efficency and brightness temperature scaling factor as in the example presented in Figure 1. That means, these instrument characteristics are consistently retrieved and did not change during the evaluated period. The tangent altitude offset Δh_{alt} varies with each retrieval, because of the rolling movement of the space shuttle. The diagonal elements of the averaging kernel matrix which belong to the critical instrument parameters are all equal one.

Retrieval of Three Data Sets

We retrieved temperature profiles for three data sets at different geographical locations. The data are recorded on 31 March 1992, over a tropical region (Atlantic–Africa), over the South Atlantic and over North America, respectively. The time of all measurements is between 3 to 6 am GMT. The NCEP analysis data are given for GMT noon time. The profile discussed in detail above and presented in Figure 1 is taken out of the South Atlantic data set.

Each retrieved single profile has been retrieved from the whole down- and up-scan of one scan cycle, i.e., within the examined altitude range each profile comes from the same number of measurements. We use only scans in this analysis for which the roll movement of the space shuttle is constant, so that it can be easily corrected and does not effect the retrieval results. The displayed vertical range in the figures is limited to a maximum altitude of 40 km (2.9 hPa), since not

all measurements have sufficiently large averaging kernels above 40 km (2.9 hPa). The top plot in Figure 3, Figure 4 and Figure 5 displays the track of the 20 km tangent point for the retrieved temperature profiles. In the retrieval shown in Figure 5, we used only a subset of the sequential measurements. The second plot of each figure shows the retrieved MAS temperature profiles as a function of latitude. For comparison, the third plot in each figure contains the NCEP temperatures. Both the MAS and the NCEP contour plots contain a row of markers (at 2.7 hPa, which is the low-pressure side of the plots) giving the positions of the MAS measurements. The fourth plot in each figure shows the differences of the MAS and NCEP data. The color scale is the same in all plots. The differences plots have a color offset relative to the MAS and NCEP data plots. Each color level corresponds to a 5 K temperature difference.

The comparison of the MAS and NCEP data shows some good consistency in basic features, but a much higher latitudinal variability in the MAS data. The MAS data are not vertically smoothed and contain structures due to noise. The residual plots show a tendency of the MAS data to lower tropopause temperatures. Since the averaging kernels in the tropopause are small (see Figure 2), these structures could be artifacts. Also, the restriction to a 5 km spaced vertical grid will usually exaggerate profile extrema [*Wehr* , 1996]. However, with this MAS data analysis the possibility of too high NCEP temperatures in the tropopause and lower stratosphere should be considered as well. One reason might be a broader vertical smoothing in the NCEP data, which smoothes out the temperature minima in the tropopause much stronger than MAS. This is supported by comparing the MAS-NCEP difference plots of the North America results versus the two other results over Atlantic-Africa and South Atlantic. The agreement of MAS and NCEP is much higher over North America, which can be seen in Figure 5 versus Figures 3 and 4. The NCEP analysis should be best over North America because numerous radiosonde profiles are available there for the NCEP analysis.

The MAS temperatures of the middle stratosphere show fine structures which are mostly within the noise error bars. Compared to the NCEP data, some local structures can be resolved which are not found in the NCEP data. For example, in Figure 3, the MAS vertical temperature gradient in the 20-40 km (54-2.9 hPa) range is not as constant as shown in the NCEP data. Evidently, both the MAS and NCEP temperatures show the same latitudinal gradient in the 15-20 km (127-54 hPa) altitudes.

Figure 4 shows a latitudinal wave structure in the MAS data over the range -20° to 0° and 25-40 km (24.5-2.9 hPa), which is missing in the NCEP temperatures. These wave structures are believed to be real because of the latitudinal phase propagation. Around -30° the MAS temperatures show stronger oscillations, especially above 30 km (11.5 hPa), where temperatures jump between the individual profiles. Therefore, it is not clear if these oscillations are real or cause by some systematical problems in these particular spectra, since the magnitude of these variations are significantly larger than the measurement noise. The latitudinal gradient in the lower stratosphere is consistent in both data sets. The residuals in the latitude range -40° to -25° indicate some systematic structures. This might be caused by either insufficient vertical resolution of the MAS retrieval or overly smooth vertical NCEP temperature gradients. Similar structures are found in the residuals of Figure 3.

The latitudinal temperature gradient over North America (Figure 5) is similar for both the MAS and NCEP temperatures. As in the prior two data sets, the MAS results show much more local structure. In particular, the lower stratosphere at low latitudes and the upper stratosphere at high latitudes is significantly colder in the MAS data.

Preliminary retrieval results of the data set "Atlantic-Africa" are published by *Wehr et al.* [1997]. These data are revised in this publication after the retrieval algorithm has been improved. In particular, in the previous analysis, the continuum has not been subtracted from the measurement and from the synthetic data, as described above. In the new analysis, presented here, the residuals between MAS and NCEP temperatures are smaller. Especially in the lower stratosphere we observe residuals of up to 10 K smaller than before. Also, both the vertical and latitudinal MAS temperature gradients have become much smoother.

Summary

Stratospheric temperatures have been successfully retrieved from MAS measurements. The values of the sideband efficiency and brightness temperature scaling are found to be consistent with the previous analysis of *Berg* [1996]. While in the previous analysis the instrument parameters have been fitted to synthetic brightness temperatures of model atmosphere profiles, they have been retrieved in this analysis simultaneously with the retrieval of atmospheric profiles.

The sideband efficiency of the MAS has been re-

trieved consistently for all measurements evaluated in this analysis. It has been found that the MAS is operating as a double sideband receiver with a slight frequency dependence of the sideband efficiency. Uncertainties in the scaling of the measured brightness temperatures, probably due to uncertainties in the antenna pattern, have been fixed by introducing a brightness temperature scaling factor. This factor has been retrieved consistently over all evaluated measurements.

Stratospheric temperatures have been retrieved on a 5 km vertical grid with reliable values in the altitude range of 15 km (127 hPa) to 40 km (2.9 hPa). Compared to the NCEP analysis data the MAS temperatures show a higher variability, since no latitudinal smoothing has been applied. We also found the tendency that MAS measures lower temperatures in the lower stratosphere, compared to NCEP. The statistical errors range from 2 K to 4 K.

The MAS has been proven to be very useful for global stratospheric temperature measurements. It precisely measures stratospheric temperature and pressure profiles with a vertical resolution of 5 km. This can certainly be used as a very valuable input to global dynamical models.

Acknowledgments. The authors would like to acknowledge the MAS team, especially the groups of G. Hartmann (PI), Max-Planck-Institut für Aeronomie, Germany, N. Kämpfer (Co-PI), University of Bern, Switzerland, R. Bevilacqua (Co-PI), Naval Research Laboratory, USA, C.L. Croskey, The Pennsylvania State University, USA, and J. Olivero, Embry Riddle Aeronautical University, USA.

Special thanks also to our colleague Arend Berg.

References

Aellig, C.P., N. Kämpfer, C. Rudin, R.M. Bevilacqua, W. Degenhardt, P. Hartogh, C. Jarchow, K. Künzi, J.J. Olivero, C. Croskey, J.W. Waters, H.A. Michelsen, Latitudinal distribution of upper stratospheric ClO as derived from space borne microwave spectroscopy, *Geophysical Research Letters, 23*, 17, 2321–2324, 1996 a.

Aellig, C.P., J. Bacmeister, R.M. Bevilacqua, M. Daehler, D. Kriebel, T. Pauls, D. Siskind, N. Kämpfer, J. Langen, G. Hartmann, A. Berg, J.H. Park, J.M. Russell III, Spaceborne H_2O observations in the Arctic stratosphere and mesosphere in the spring of 1992, *Geophysical Research Letters, 23*, 17, 2325–2328, 1996 b.

Berg, A., Bestimmung des atmosphärischen Druckes mit Hilfe von satellitengetragener passiver Mikrowellenradiometrie, PhD thesis, *Verlag Shaker, Aachen, Germany*, 1996.

Bevilacqua, R.M., D.L. Kriebel, T.A. Pauls, C.P. Aellig, D.E. Siskind, M. Daehler, J.J. Olivero, S.E. Puliafito, G.K. Hartmann, N. Kämpfer, A. Berg, C.L. Croskey, MAS measurements of the latitudinal distribution of water vapor and ozone in the mesosphere and lower thermosphere, *Geophysical Research Letters, 23*, 17, 2317–2320, 1996.

Croskey, C.L., N. Kämpfer, R.M. Bevilacqua, G. Hartmann, K. Künzi, P. Schwartz, J. Olivero, S. Puliafito, C. Aellig, G. Umlauft, W. Waltman, W. Degenhardt, The Millimeter Wave Atmospheric Sounder (MAS): A Shuttle–based remote sensing experiment, *IEEE Transactions on Geoscience and Remote Sensing, 40*, 1090-1100, 1992.

Fishbein, E.F., R.E. Cofield, L. Froideveaux, R.F. Jarnot, T. Lungu, W.G. Read, Z. Shippony, J.W. Waters, I.S. McDermid, T.J. McGee, U. Singh, M. Gross, A. Hauchecorne, P. Keckhut, M.E. Gelman, R.M. Nagatani, Validation of UARS Microwave Limb Sounder temperature and pressure measurements, *Journal of Geophysical Research, 101*, D6, 9983–10016, 1996.

Fleming, E.L., S. Chandra, M.R. Shoeberl, J.J. Barnett, Monthly Mean Global Climatology of Temperature, Wind, Geopotential Height, and Pressure for 0 – 120 km, NASA Technical Memorandum 100687, February 1988.

Hartmann, G.K., W. Degenhardt, M.L. Richards, H.J. Liebe, G.A. Hufford, M.G. Cotton, R.M. Bevilacqua, J.J. Olivero, N. Kämpfer, J. Langen, Zeeman splitting of the 61 Gigahertz Oxygen (O_2) line in the mesosphere, *Geophysical Research Letters, 23*, 17, 2329–2332, 1996 a.

Hartmann, G.K., R.M. Bevilacqua, P.R. Schwartz, N. Kämpfer, K.F. Künzi, C.P. Aellig, A. Berg, W. Boogaerts, B.J. Connor, C.L. Croskey, M. Daehler, W. Degenhardt, H.D. Dicken, D. Goldizen, D. Kriebel, J. Langen, A. Loidl, J.J. Olivero, T.A. Pauls, S.E. Puliafito, M.L. Richards, C. Rudin, J.J. Tsou, W.B. Waltman, G. Umlauft, R. Zwick, Measurements of O_3, H_2O and ClO in the middle atmosphere using the millimeter-wave atmospheric sounder (MAS), *Geophysical Research Letters, 23*, 17, 2313–2316, 1996 b.

Kaye, J.A., T. Miller, The ATLAS Series of Shuttle Missions, *Geophysical Research Letters, 23*, 17, 2285–2288, 1996.

Langen, J., A. Berg, H.D. Dicken, T. Wehr, W. Degenhardt, N. Kämpfer, R. Bevilacqua, Pressure profiles of the middle atmosphere retrieved from Millimeter-Wave Atmospheric Sounder (MAS) on board the Space Shuttle mission ATLAS-1, IGARSS Symposium Digest WP.T.05, Pasadena (USA), 1994.

Liebe, H.J., P.W. Rosenkranz, G.A. Hufford, Atmospheric 60-GHz Oxygen Line Spectrum: New Laboratory Measurements and Line Parameters, *Journal of Quantitative Spectroscopy and Radiative Transfer*, 48, 629–643, 1992.

Olivero, J.J., T.A. Pauls, R.M. Bevilacqua, D. Kriebel, M. Daehler, M.L. Richards, N. Kämpfer, A. Berg, C. Stodden, Distinctive ozone structure in the high-latitude stratosphere: Measurements by the Millimeter-wave Atmospheric Sounder, *Geophysical Research Letters, 23*, 17, 2309–2311, 1996.

Rodgers, C.D., Retrieval of atmospheric temperature and composition from remote measurements of thermal radiation, *Reviews of Geophysics and Space Physics, 14*, (4), 609–624, 1976.

Waters, J.W., D.H. Staelin, K.F. Künzi, R.L. Pettyjohn, R.K.L. Poon, Microwave remote sensing of atmospheric temperature profiles from the NIMBUS 5 Microwave Satellite, *Space Res.*, vol. XV, p. 117, 1975.

Wehr, T., Inversion atmosphärischer Parameter aus Submillimeter- und Millimeterwellen-Spektren, PhD thesis, Library of the University of Bremen, Germany, 1996.

Wehr, T., S. Bühler, A. von Engeln, J. Langen, K. Künzi, Measurements of stratospheric temperature with a space borne microwave limb sounding instrument, *Atmospheric Ozone — Proc. Ozone Symp. L'Aquila — 1996,* R.D. Bojkov and G. Visconti Eds., Italy, 1003–1006, 1997.

T. Wehr, University of Maryland Baltimore County, Department of Physics, 1000 Hilltop Circle, Baltimore, MD 21250, USA

K. Künzi, S. Bühler, A. von Engeln, University of Bremen, Institute of Environmental Physics, P.O. Box 330440, 28334 Bremen, Germany

J. Langen, ESA-ESTEC VRA, Postbus 299, NL 2200 AG Noordwijk, The Netherlands

September 17, 1997; revised ?; accepted ?.

This preprint was prepared with AGU's LaTeX macros v4. File paper˙agupp formatted July 22, 1998.

With the extension package 'AGU^{++}' by P.W.Daly, version 1.5 from 1996/08/20

Figure 1. Retrieval results of atmospheric temperature in the altitude range of 10-60 km (281-0.2 hPa), upper plot, and instrument parameters, lower plots. Lower left plot: The sideband efficiency has been retrieved as a linear function of frequency, independently for each of the three oxygen lines. The $\diamond$ symbol shows the a priori value of the sideband efficiency, at the first and last measured point of each line. The + symbol shows the retrieval result.

Figure 2. Left figure: the statistical errors of the temperature profile. The dotted line shows the smoothing error, the dashed line the measurement error (noise) and the solid line the total statistical error, in terms of the square roots of the diagonal elements of the total statistical error covariance matrix. This matrix is the sum of the smoothing error covariance matrix and the measurement error covariance matrix. Right figure: the rows of the averaging kernel matrix. The plotted altitude range is 10-60 km (281-0.2 hPa).

Figure 3. Flight over Atlantic–Africa: flight track, MAS measurement, NCEP data, residuals. Each color level corresponds to a 5 K temperature difference. The altitude range is 15-40 km (127-2.9 hPa).

Figure 4. Flight over the South Atlantic: flight track, MAS measurement, NCEP data, residuals. Each color level corresponds to a 5 K temperature difference. The altitude range is 15-40 km (127-2.9 hPa).

Figure 5. Flight over North America: flight track, MAS measurement, NCEP data, residuals. Each color level corresponds to a 5 K temperature difference. The altitude range is 15-40 km (127-2.9 hPa).

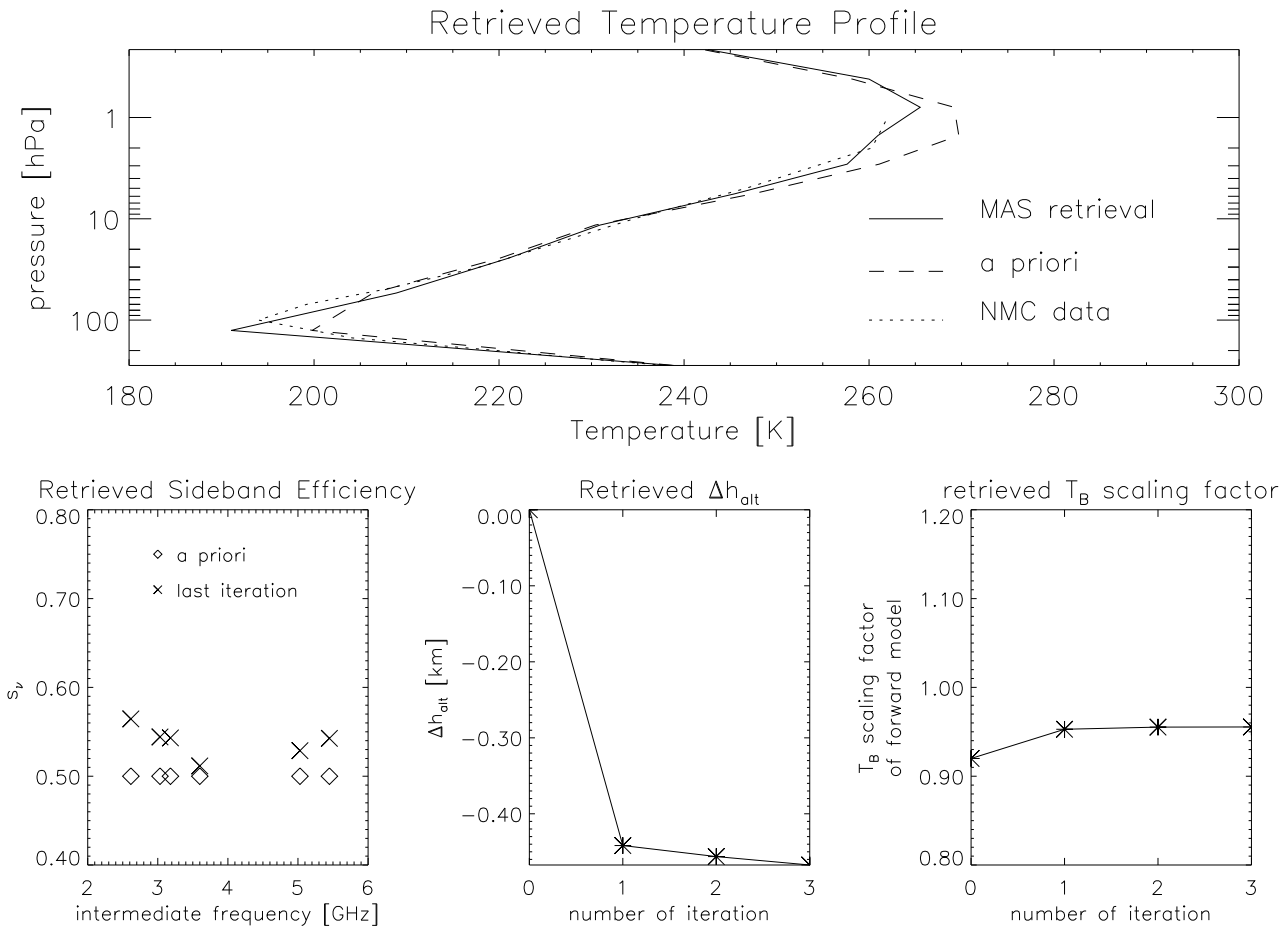
Retrieved Temperature Profile
pressure [hPa]
1
10
100
180
200
220
240
260
280
300
Temperature [K]
MAS retrieval
a priori
NMC data
Retrieved Sideband Efficiency
a priori
last iteration
s_ν
0.80
0.70
0.60
0.50
0.40
2
3
4
5
6
intermediate frequency [GHz]
Retrieved Δh_{alt}
Δh_{alt} [km]
0.00
−0.10
−0.20
−0.30
−0.40
0
1
2
3
number of iteration
retrieved T_B scaling factor
T_B scaling factor of forward model
1.20
1.10
1.00
0.90
0.80
0
1
2
3
number of iteration

Figure 1.

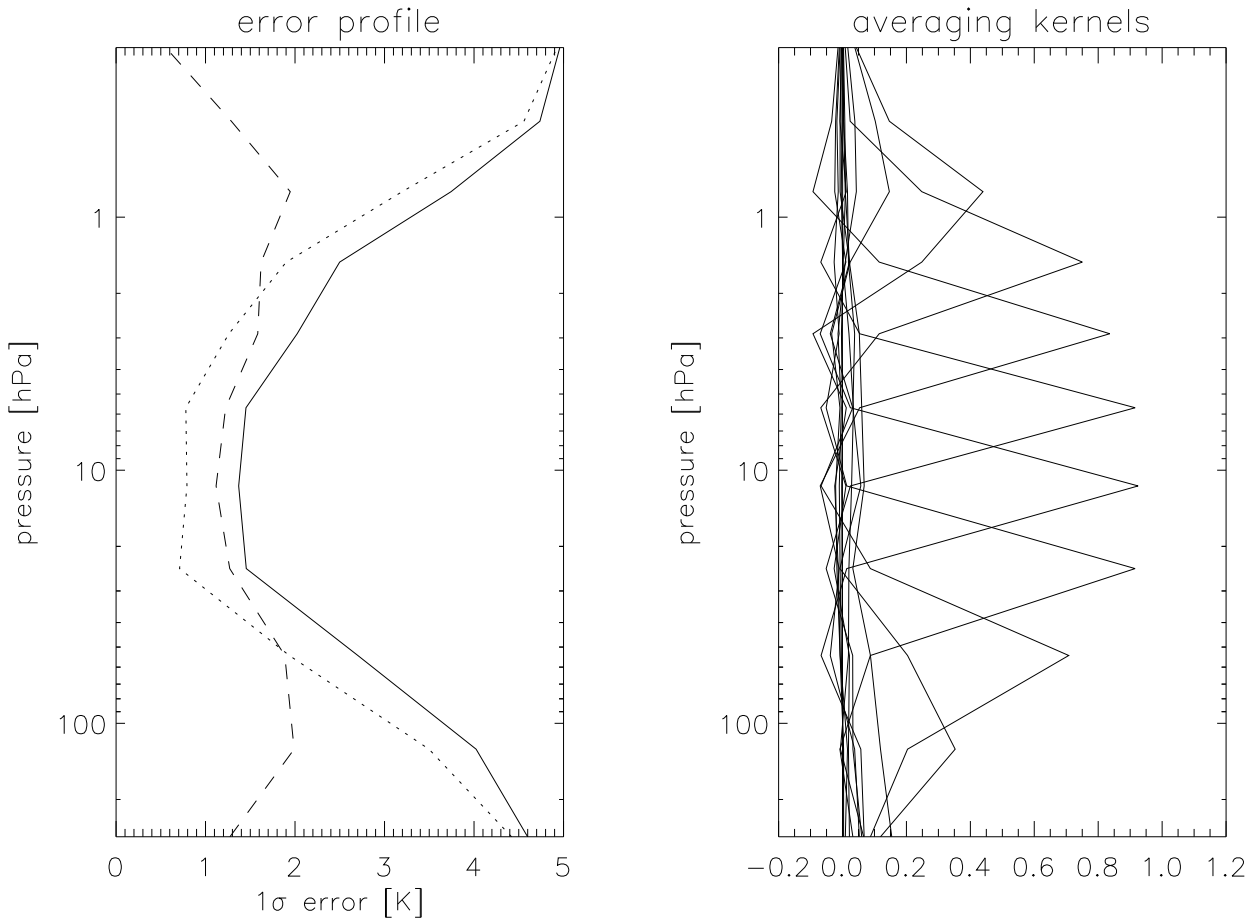
error profile
averaging kernels
pressure [hPa]
1
10
100
0
1
2
3
4
5
1σ error [K]
−0.2
0.0
0.2
0.4
0.6
0.8
1.0
1.2

Figure 2.

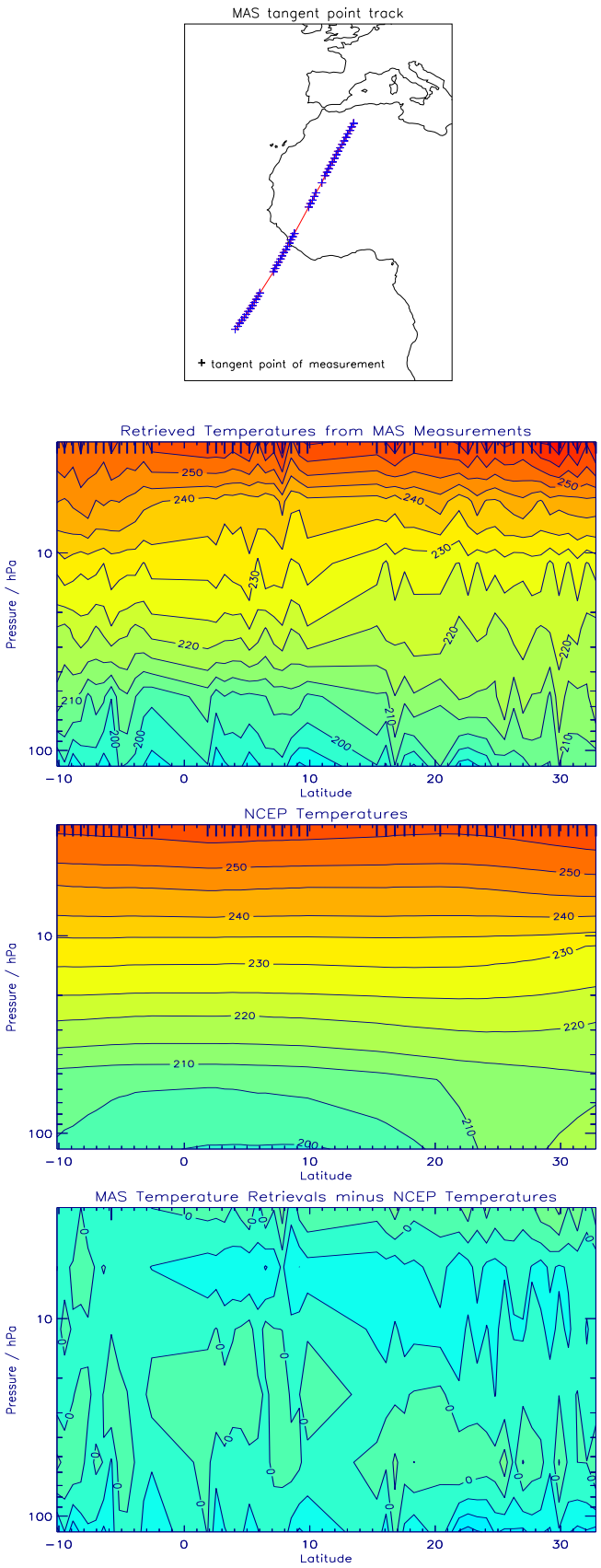
MAS tangent point track
+ tangent point of measurement
Retrieved Temperatures from MAS Measurements
NCEP Temperatures
MAS Temperature Retrievals minus NCEP Temperatures
Pressure / hPa
Latitude
10
100
−10
0
10
20
30
250
240
230
220
210
200

Figure 3.

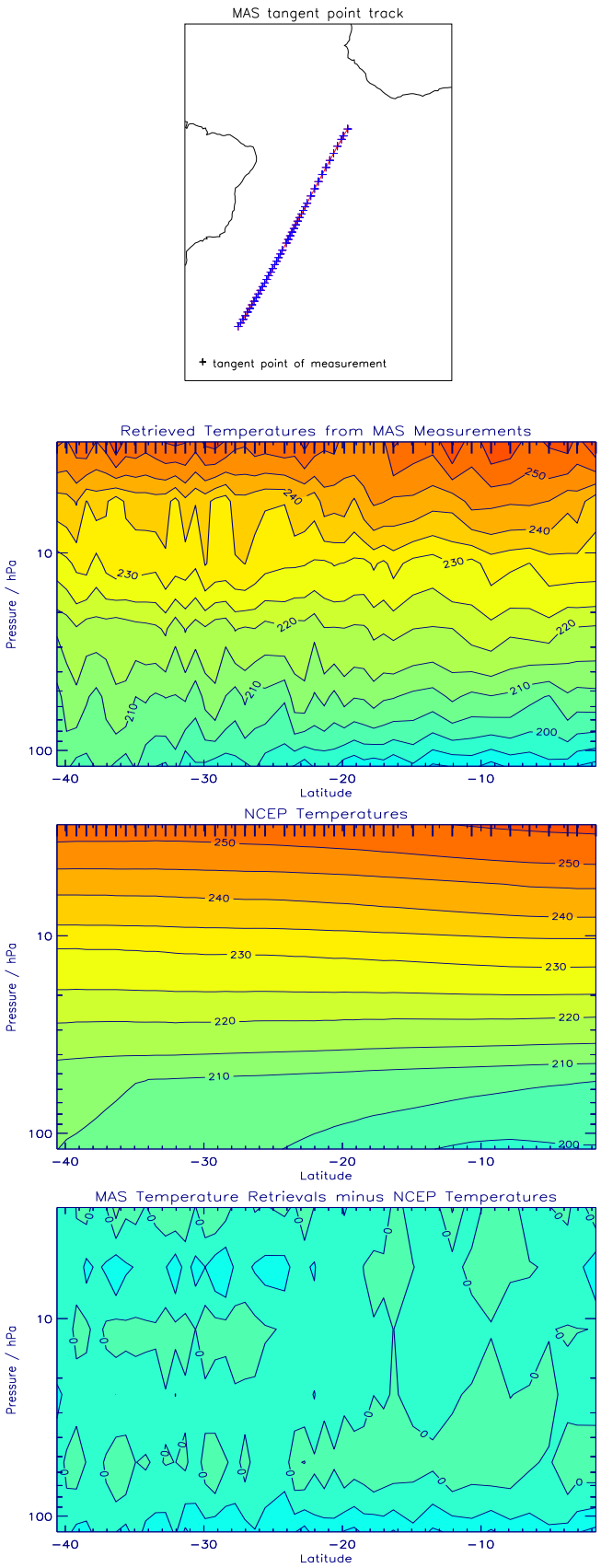
MAS tangent point track
+ tangent point of measurement
Retrieved Temperatures from MAS Measurements
NCEP Temperatures
MAS Temperature Retrievals minus NCEP Temperatures
Pressure / hPa
Latitude
10
100
−40
−30
−20
−10
250
240
230
220
210
200

Figure 4.

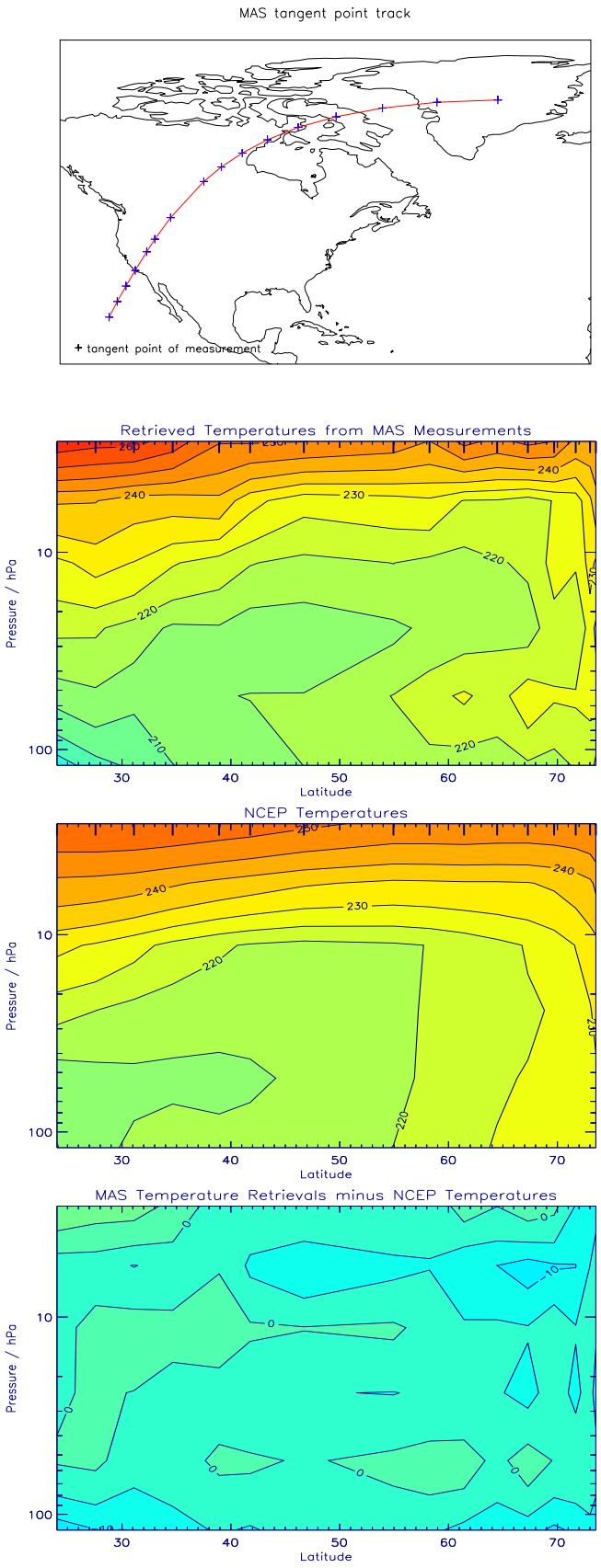
MAS tangent point track
+ tangent point of measurement
Retrieved Temperatures from MAS Measurements
NCEP Temperatures
MAS Temperature Retrievals minus NCEP Temperatures
Pressure / hPa
Latitude
10
100
30
40
50
60
70
210
220
230
240

Figure 5.